The C-terminus of stathmin-like proteins governs the stability of their complexes with tubulin

Valérie Campanacci, Benoît Gigant

The C-terminus of stathmin-like proteins governs the stability of their complexes with tubulin.

Valérie Campanacci, Benoît Gigant[#]

Université Paris-Saclay, CEA, CNRS, Institute for Integrative Biology of the Cell (I2BC), 91198, Gif-sur-Yvette, France.
Correspondence to benoit.gigant@i2bc.paris-saclay.fr (BG).

Microtubule dynamics is modulated by many cellular factors including stathmin family proteins. Vertebrate stathmins sequester two αβ-tubulin heterodimers into a tight complex that cannot be incorporated in microtubules. Stathmins are regulated at the expression level during development and among tissues; they are also regulated by phosphorylation. Here, we study the dissociation kinetics of tubulin:stathmin assemblies in presence of different tubulin-binding proteins and identify a critical role of the C-terminus of the stathmin partner. Destabilizing this C-terminal region may represent an additional regulatory mechanism of the interaction with tubulin of stathmin proteins.

Keywords
CPAP; CopN; Fluorescence spectroscopy; Microtubule dynamics regulation; Stathmin-like RB3; Tubulin-binding proteins

Highlights

- Stathmin proteins bind to tubulin to form stable sequestering complexes.
- Interfering with the stathmin C-terminus destabilizes the association with tubulin.
- Identification of a new mechanism for the regulation of stathmin proteins.

Microtubules are dynamic assemblies of αβ-tubulin heterodimers that are involved in important processes in eukaryotic cells, such as ciliogenesis, intracellular transport and mitosis. To fulfill these different functions, microtubule dynamics is modulated by several families of proteins which can be broadly classified into polymerases, depolymerases, microtubule stabilizers and microtubule destabilizers, including tubulin sequestering molecules (1–3).
Stathmin is the main tubulin sequestering protein in vertebrates. Initially proposed to be involved in diverse regulatory pathways in response to extracellular signals (4), stathmin was

later identified as a microtubule destabilizing factor (5), forming a tight complex with two protofilament-like tubulin molecules which become incompetent for microtubule assembly (6, 7). Although a direct microtubule destabilizing effect of stathmin has been proposed (8, 9), its intracellular concentration (up to 10 μM (10)) as compared to that of tubulin (about 24 μM (11)) is compatible with a pure tubulin-sequestering activity (6, 12). Whereas stathmin is present in many cells, its expression is highly variable during development and among tissues (13), constituting a first level of regulation. It is also regulated by phosphorylation on four serine residues, which lowers the affinity for tubulin (12, 14, 15) hence favors microtubule assembly. This ability to bind tubulin is shared by the other stathmin family members, all comprising a C-terminal semi-conserved stathmin-like domain (SLD) (16, 17). In addition, they have palmitoylated N-terminal extensions, which target them to membranes (18), whereas stathmin is cytosolic. Another difference with stathmin is that the other family members are found solely in the nervous system (16, 19). The SLD can be subdivided into an N-terminal β-hairpin motif, which caps α-tubulin at one end of the complex, and a long C-terminal α-helix interacting with the two tubulin molecules of the tubulin:SLD 2:1 ternary complex (T_2SLD), both elements being connected by a more variable linker (20). The stability of T_2SLD complexes however varies (16), and their regulation by phosphorylation displays both similarities and specificities (16, 21).

CPAP is a centrosomal protein which controls the length of centrioles (22–24). It comprises a microtubule-destabilizing domain, named PN2-3 and containing the 311 to 422 CPAP residues (25). It has been observed in a surface plasmon resonance experiment that PN2-3 enhances the release of tubulin bound to immobilized SLD (26). Here, we show that PN2-3 greatly accelerates the dissociation of tubulin:SLD complexes in solution. Taking advantage of the recently determined tubulin:PN2-3 structure (27), we propose that this remarkable behavior results from the interference of PN2-3 with the SLD C-terminus, a model that we then tested experimentally using proteins targeting different tubulin surfaces. This mechanism may represent an efficient and rapid way for the cell to disrupt T_2SLD complexes, hence to modulate microtubule assembly, in addition to a phosphorylation-based regulation.

Results and Discussion

We previously observed that the detachment of tubulin bound to immobilized $RB3_{SLD}$ (i.e. the SLD of stathmin 4, also known as RB3) is accelerated in presence of PN2-3 (26). Unfortunately, in part because high resolution structural data on tubulin:PN2-3 were not available, these surface plasmon resonance results did not lead to a mechanistic model. To achieve this goal,

we first investigated the effect of PN2-3 on the tubulin:$RB3_{SLD}$ 2:1 complex (T_2R) in solution. We produced an acrylodan-labeled $RB3_{SLD}$ derivative and a fluorescent signal slowly developed upon addition of tubulin to this protein (Fig. 1). Adding excess unlabeled $RB3_{SLD}$ to fluorescent T_2R led to a slow decrease of the signal, from which a k_{obs} of (1.1 ± 0. 2) x 10^{-3} s^{-1} (mean ± s.d., here and throughout) can be extracted. This value is an estimate of the dissociation rate constant (k_{off}) and is in good agreement with previous results (28). By contrast, upon addition of excess PN2-3 (or of shorter 316-397 or 321-397 CPAP fragments), the fluorescence signal went back to the basal value within the mixing time of the solution (estimated to be 10 seconds at most), indicating an active dissociation of T_2R by PN2-3 (Fig. 1). Therefore, this experiment emphasizes the slow kinetics of association and dissociation of the tubulin:$RB3_{SLD}$ interaction, as also found by fluorescence correlation spectroscopy (28), and highlights the strong destabilization of the resulting T_2R complex by PN2-3.

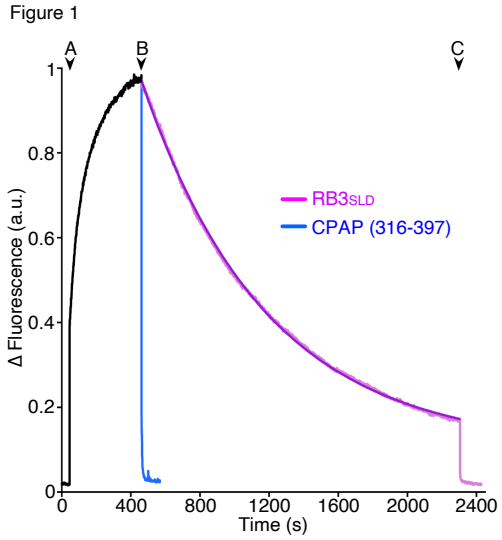

Figure 1. PN2-3 based constructs of CPAP destabilize the T_2R complex. Tubulin (200 nM) was added to a 80 nM acrylodan-labeled $RB3_{SLD}$ solution (point A). At point B, 4 µM of either unlabeled $RB3_{SLD}$ (pink curve) or CPAP 316-397 construct (blue) were added. Point C corresponds to the addition of 4 µM CPAP construct to the "$RB3_{SLD}$" sample. The magenta curve is the fit with a mono-exponential decay function of the signal decrease upon addition of excess $RB3_{SLD}$ to the fluorescent complex. a.u., arbitrary units.

A first possibility to explain this last feature would be that PN2-3 stabilizes a tubulin conformation which would be less favorable for SLD binding. However, the structure of tubulin bound to PN2-3 based constructs does not support this hypothesis (27). Indeed, superposing the α and β tubulin subunits in these complexes (e.g. pdb id 7Q1F) to those of T_2R (pdb id 3RYC) led to root mean square deviations of 0.82 Å (α-tubulin, 427 Cαs compared) and 0.42 Å (β-

tubulin, 429 Cαs compared), respectively, indicating highly similar conformations. In addition, the angle between α- and β-tubulin in the different tubulin:CPAP structures we determined varies between 11.6° and 14.3° (27), within the values observed in crystal structures of tubulin complexes (29), including T_2R (20), as well as in soluble, isolated tubulin (30). We conclude that PN2-3 based fragments do not destabilize T_2R by inducing a conformational change in tubulin.

Because PN2-3 interacts with the longitudinal surface of β-tubulin (27), a second possibility would be that it destabilizes T_2R by targeting the β subunit surface engaged in tubulin:tubulin contacts within this complex (17, 20) (Fig. 2A). This hypothesis predicts that PN2-3 will not enhance the dissociation of tubulin:R1, R1 being an artificial SLD engineered to bind one tubulin heterodimer (Fig. 2A) (31). We actually found the opposite: adding excess PN2-3 to fluorescent tubulin:R1 led to an ~800-fold enhanced dissociation of this complex compared to the addition of unlabeled R1 (Fig. 2B). Fitting the data with a mono-exponential decay function led to a poor fit. It was improved using a double-exponential decay function (Fig. S1), suggesting a scheme according to which PN2-3 binds to tubulin:R1 to form an unstable [PN2-3:tubulin:R1] assembly from which R1 rapidly dissociates.

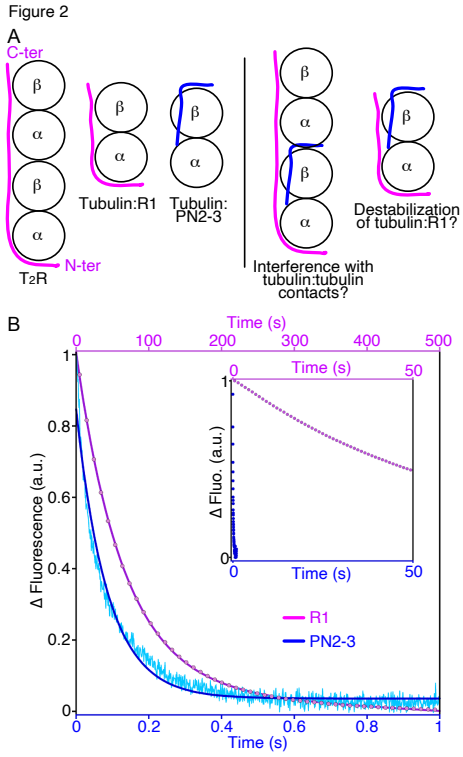

Figure 2. PN2-3 enhances the dissociation of R1 from tubulin. (**A**) Hypothesis on the destabilization of T_2R by PN2-3. (Left) Schematic representation of T_2R (with the N- and C-terminal ends of $RB3_{SLD}$ labeled), of tubulin:R1 and of tubulin:PN2-3. The SLDs are in pink,

PN2-3 is in blue. (Right) PN2-3 might destabilize T_2R by targeting the β-tubulin surface engaged in tubulin:tubulin contacts within the complex, leading to steric conflicts with the α subunit of the second tubulin molecule. According to this hypothesis, PN2-3 is not expected to enhance the dissociation of tubulin:R1 (whether it competes with R1 for tubulin binding or not). (**B**) PN2-3 destabilizes tubulin:R1. PN2-3 (2 μM) or R1 (2.1 μM) was added to fluorescent tubulin:R1 obtained by mixing 30 nM acrylodan-labeled R1 with 50 nM tubulin. The fluorescence decrease was monitored in a stopped-flow apparatus during one second in the case of added PN2-3 (light blue noisy curve) or 500 s in the case of R1 (pink dots, 5% of the experimental data points are shown). The data were fit with a mono-exponential decay function, which also comprised a photobleaching term in the case of R1. The fitting leads to a k_{obs} of 0.017 ± 0.002 s^{-1} with added unlabeled R1 (similar to a previous estimate (31)) and a k_{obs} of 13.7 ± 3.5 s^{-1} with added PN2-3. The fitted curves are in magenta and in blue, respectively. (Inset) The two kinetics presented on the same time scale. Experimental data points are displayed as blue or pink dots, 10% or 50% of which are shown, in the case of PN2-3 or R1, respectively.

A third possibility would be that PN2-3 proceeds by interfering with the SLD partner of transient [PN2-3:tubulin:SLD] complexes. Indeed, modeling PN2-3 based CPAP fragments on the distal β-tubulin subunit of T_2R indicates that there would be steric conflicts with the SLD α-helix C-terminus, which interacts with this distal β subunit (Fig. 3A). A mechanism based on the destabilization of this SLD region would agree with the observation that the SLD of RB3', a splice variant of RB3 in which the last 19 residues are replaced by a shorter stretch of 6 residues (19), makes a less stable assembly with tubulin as evaluated by size-exclusion chromatography (16). It would also be consistent with the tight complex R1 makes with tubulin compared to constructs of similar length but which do not include the C-terminal stabilizing motif of $RB3_{SLD}$ present in R1 (31). This hypothesis predicts that proteins whose binding site on tubulin overlaps with that of the SLD C-terminus should enhance the dissociation of tubulin:SLD complexes, whereas proteins targeting other regions of the SLD binding site on tubulin should not (or if so not by the same mechanism). Proteins of the former category include CopN from the bacterial pathogen *Chlamydia pneumoniae* (32), whereas the motor domain of kinesins (33) and the artificial α-tubulin specific iE5 αRep protein (29) belong to the second one (Fig. 3B). The effect on T_2R stability of these three proteins was evaluated in the fluorescence chase experiment.

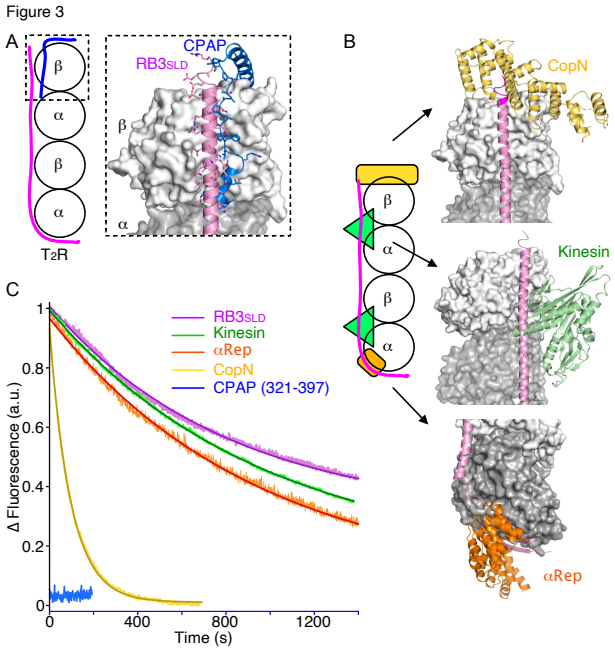

Figure 3. Interfering with the SLD C-terminus enhances the dissociation of T_2R. (**A**) The modeling of a PN2-3 based fragment (pdb id 7Q1F (27)) on the distal β subunit of T_2R (pdb id 3RYC (37)) indicates that the binding of PN2-3 to T_2R would lead to steric conflicts with the RB3 region interacting with this β-tubulin. (**B**) Modeling CopN (pdb id 6GX7 (32)) on the distal β subunit of T_2R predicts that CopN interferes with the C-terminus of the SLD α-helix, whereas modeling a kinesin motor domain (pdb id 4LNU (38)) or the iE5 αRep (pdb id 6GWC (29)) on T_2R suggests a "more classical" competition mechanism. The C-terminal residues absent in the $RB3_{SLD}$ 139Stop construct are highlighted in magenta in the top panel. (**C**) Adding 4 µM kinesin (green curve) or 4 µM iE5 αRep (orange) to a solution containing 80 nM acrylodan-labeled $RB3_{SLD}$ and 200 nM tubulin leads to a fluorescence decrease kinetics which is similar to that of the control chase experiment with 4 µM $RB3_{SLD}$ added (pink). By contrast, adding 4 µM CopN (yellow) leads to a ~10-fold faster dissociation of T_2R. The noisy curves represent the time course of fluorescence change, whereas darker smooth curves represent fitted curves with a mono-exponential decay function from which apparent k_{obs} of (2.0 ± 1.6) x 10^{-3} s^{-1} (kinesin), (1.3 ± 0.2) x 10^{-3} s^{-1} (αRep) and (10.0 ± 0.8) x 10^{-3} s^{-1} (CopN) can be extracted, compared to (1.1 ± 0.2) x 10^{-3} s^{-1} in the case of $RB3_{SLD}$. In presence of excess 321-397 CPAP construct (blue), the signal decrease is too fast to be recorded by this method, and the apparent k_{obs} is estimated to be > 0.1 s^{-1} (Fig. S2A).

The addition of excess kinesin or iE5 αRep to fluorescent T_2R led to kinetics similar to the one when unlabeled $RB3_{SLD}$ was added as a competitor (Fig. 3C), showing that these proteins

compete with $RB3_{SLD}$ for tubulin binding, as expected (Fig. 3B), but do not substantially destabilize preformed T_2R. By contrast, the dissociation of $RB3_{SLD}$ from tubulin was enhanced about 10-fold in presence of CopN, indicating a destabilization of the T_2R complex by this protein (Fig. 3C). Interestingly, CopN was less efficient than PN2-3 based fragments, with the ratio between the apparent k_{obs} for T_2R dissociation in presence of PN2-3 or of CopN expected to be > 10 (Fig. S2A). Although CopN has a slightly lower affinity for tubulin than CPAP constructs (dissociation constants estimated to be 50 and 15 nM, respectively, (27, 32)), the concentration used in the chase experiment (4 μM, far above the dissociation constants) ensured that the efficiency difference in destabilizing T_2R did not result from the gap in affinity for tubulin. Moreover, the two following experiments suggest that it is not explained either by a difference in affinity for T_2R. First, doubling the concentration of CopN in the chase experiment (8 μM instead of 4 μM) did not change the dissociation kinetics of T_2R (Fig. S2B). Second, a 321-397 CPAP fragment having the E323R, E324R and I327R substitutions, which decrease about 20-fold the affinity for tubulin (27), hence which presumably also affect the affinity for T_2R, behaved as the unmodified construct in our assay (Fig. S2B). Therefore, we conclude that PN2-3 is inherently more effective than CopN to destabilize tubulin:stathmin complexes, possibly because it would be in steric conflict with a longer segment of the SLD C-terminus in transient complexes with tubulin (Fig. 3A,B).

The experiments with CPAP constructs and with CopN added to T_2R support a mechanism based on the destabilization of the C-terminus of the SLD α-helix. Another way to disrupt the SLD C-terminus and its interaction with tubulin would be to shorten it. To this end, we generated a C-terminal truncated $RB3_{SLD}$ by introducing a stop codon at position 139 (illustrated in the top panel of Fig. 3B; numbering is in reference to stathmin (16)). Adding excess $RB3_{SLD}$ as a competitor, we found that the dissociation of tubulin from this RB3 truncated mutant is about 5-fold faster than that from the parental construct (Fig. 4). This feature was further ascertained using kinesin in the chase experiment (Fig. 4). It also agreed with a preliminary and more qualitative characterization based on a size-exclusion chromatography analysis of tubulin:$RB3_{SLD}$ 139Stop complexes (31). Remarkably, we did not find such a difference upon addition of excess CopN, the apparent k_{obs} for the dissociation of tubulin bound to either full length $RB3_{SLD}$ or the shorter 139Stop construct being similar in this case (Fig. 3C and 4). This last result indicates that the destabilizing effects of CopN and of the shortening of the SLD C-terminus are not additive. It suggests that both operate through the same mechanism, i.e. the disruption of the interactions of the SLD C-terminal region with tubulin.

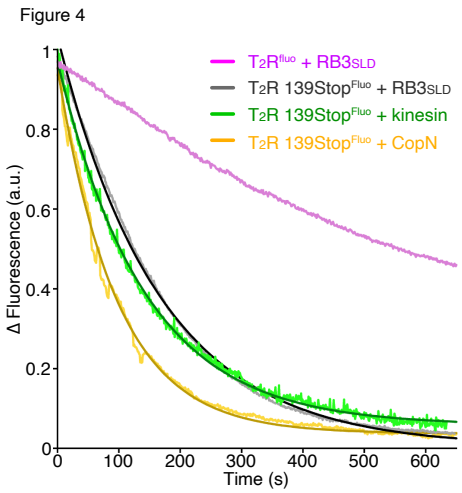

Figure 4. **The $RB3_{SLD}$ 139Stop mutant makes a less stable complex with tubulin than wild type $RB3_{SLD}$.** To fluorescent tubulin:$RB3_{SLD}$ 139Stop complex (obtained by mixing 80 nM acrylodan-labeled $RB3_{SLD}$ 139Stop with 200 nM tubulin), the addition of excess $RB3_{SLD}$ (grey curve) or kinesin (green) leads to a signal decrease which is faster than the one associated with the addition of $RB3_{SLD}$ to fluorescent T_2R (pink curve, data taken from Fig. 1). Fitting the experimental data points with a mono-exponential decay function (darker smooth curves) gives a k_{obs} estimate of $(5.7 \pm 1.2) \times 10^{-3}$ s^{-1} for the tubulin:$RB3_{SLD}$ 139Stop dissociation. The addition of excess CopN (yellow) leads to a kinetics with an apparent k_{obs} of $(11.5 \pm 1.5) \times 10^{-3}$ s^{-1}, similar to the situation where CopN is added to T_2R (Fig. 3C).

Conclusion.

In this report, we show that PN2-3 and related CPAP fragments destabilize tubulin:SLD complexes (Fig. 1, 2B, 3C) and that this property is shared by the bacterial protein CopN (Fig. 3C). Interestingly, both CPAP and CopN directly modulate microtubule dynamics, controlling centriolar microtubule growth (34) and interfering with microtubule nucleation and plus end elongation (32, 35), respectively. Our results indicate that they may also have an indirect effect, favoring the release of tubulin from T_2SLD complexes.

The regulation of the tubulin:SLD interaction by phosphorylation has been well documented (12, 14, 15, 21), with up to four sites clustered in the N-terminal moiety of the SLD (16) which, when phosphorylated, substantially reduce the affinity for tubulin (12, 15). It has been proposed that phosphorylation proceeds by destabilizing secondary structural elements of stathmin. In particular an N-terminal segment of its α-helix is disrupted upon Ser63 modification (15). Our results lead to a model where proteins interfering with the C-terminus of SLD α-helix, at a distance from the phosphorylation sites, also weaken the stability of tubulin:SLD complexes.

As a further consequence of this destabilization, phosphorylation of stathmin proteins could be facilitated because they are expected to be better substrates for protein kinases when they are detached from tubulin.

To summarize, targeting the SLD C-terminus might be an efficient way for the cell to release quickly tubulin bound to an SLD partner and make it available for remodeling the microtubule network, possibly in subcellular compartments (18), a mechanism which could be hijacked by the *C. pneumoniae* CopN effector. It potentially represents another regulatory mechanism for SLDs, in addition to regulations at the expression level and by phosphorylation.

Methods.

Proteins. RB3 variants were obtained by standard molecular biology techniques from $RB3_{SLD}$ (17) but with the C14A mutation (stathmin numbering). $RB3_{SLD}$ 139Stop was prepared by inserting a stop codon at position 139. For acrylodan labeling, a cysteine residue was introduced at position 72 (L72C substitution). All constructs were verified by sequencing. The $RB3_{SLD}$ proteins was produced and purified (17) and modified by acrylodan (31) following published protocols. The production and purification of R1 and its R71C variant (31), of PN2-3, of the 316-397 CPAP fragment, and of the 321-397 CPAP construct and its E323R-E324R-I327R triple mutant (26, 27), of CopN (35), of the iE5 αRep (29), and of the kinesin motor domain (33) have also been described. Tubulin was purified from ovine brain by two cycles of assembly in a high molarity pipes buffer and disassembly (36). Before use, an additional assembly and disassembly cycle was performed to remove inactive protein.

Fluorescence spectroscopy. The experiments were based on the fluorescence signal (λ_{ex} 290 nm, λ_{em} 505 nm) which develops upon addition of tubulin to acrylodan-labeled SLD (Fig. 1). They were performed at room temperature in a buffer consisted of 25 mM Pipes-K, pH 6.8, 0.5 mM $MgCl_2$, 0.2 mM EGTA, and 10 µM GDP. Unless otherwise stated, fluorescent T_2R was obtained by mixing 80 nM acrylodan-labeled $RB3_{SLD}$ with 200 nM tubulin, and the protein competitor was added at a 4 µM concentration. In the chase experiment with CopN, a test with an 8 µM concentration was also performed and led to a similar dissociation kinetics than with 4 µM CopN (Fig. S2B). In the case of the tubulin:R1 experiments (Fig. 2 and S1), the fluorescent complex was formed by adding 50 nM tubulin to 30 nM acrylodan-labeled R1, and the fluorescence decrease was recorded after addition of 2 µM PN2-3 or 2.1 µM unlabeled R1. Kinetics were recorded using a FluoroMax spectrofluorometer (Jobin Yvon, Horiba), except the experiments with tubulin:R1 which were performed using a Hi-Tech KinetAsyst stopped-

flow system (TgK Scientific). The signal decrease upon addition of a competitor to fluorescent tubulin:SLD complexes was fit either with a mono-exponential decay function, which also included a photobleaching correction if required (equation 1),

$$Fluo = Fluo_{min} + \Delta Fluo \times e^{-k_{obs} \times t} + b \times t \quad \text{(equation 1)}$$

where *Fluo* is the fluorescence signal, $Fluo_{min}$ is the fluorescence at infinite time, $\Delta Fluo$ is the amplitude of the fluorescence variation, and b is the photobleaching term, or with a double-exponential decay function (equation 2),

$$Fluo = Fluo_{min} + \Delta Fluo1 \times e^{-k_{obs1} \times t} + \Delta Fluo2 \times e^{-k_{obs2} \times t} \quad \text{(equation 2)}$$

where $\Delta Fluo1$ and k_{obs1} are associated with the first phase of the dissociation kinetics and $\Delta Fluo2$ and k_{obs2} with the second one.

Acknowledgements

We thank M. Knossow (I2BC, Gif-sur-Yvette) for discussions and for a critical reading of the manuscript. We thank J. Pernier and C. le Clainche for technical assistance in fluorescence measurements. Financial support by CNRS, by the Fondation ARC pour la Recherche sur le Cancer (Grant PJA20161204544 to B.G.), and the Agence Nationale de la Recherche (Grant ANR-22-CE11-0002-01 to B.G.) is acknowledged.

Author Contributions

V.C. and B.G. designed and performed research; B.G. analyzed data and wrote the paper with input from V.C.

References

1. A. Akhmanova and M. O. Steinmetz (2015) Control of microtubule organization and dynamics: two ends in the limelight. *Nat. Rev. Mol. Cell Biol.* **16**, 711–726
2. H. V. Goodson and E. M. Jonasson (2018) Microtubules and microtubule-associated proteins. *Cold Spring Harb. Perspect. Biol.* **10**, a022608
3. H. Bowne-Anderson et al. (2015) Regulation of microtubule growth and catastrophe: unifying theory and experiment. *Trends Cell Biol*. **25**, 769–779
4. A. Sobel (1991) Stathmin: a relay phosphoprotein for multiple signal transduction? *Trends Biochem. Sci.* **16**, 301–305
5. L. D. Belmont and T. J. Mitchison (1996) Identification of a protein that interacts with tubulin dimers and increases the catastrophe rate of microtubules. *Cell*. **84**, 623–631
6. L. Jourdain et al. (1997) Stathmin: a tubulin-sequestering protein which forms a ternary T2S complex with two tubulin molecules. *Biochemistry*. **36**, 10817–10821
7. M. O. Steinmetz et al. (2000) Op18/stathmin caps a kinked protofilament-like tubulin tetramer. *EMBO J*. **19**, 572–580
8. B. Howell et al. (1999) Dissociation of the tubulin-sequestering and microtubule catastrophe-promoting activities of oncoprotein 18/stathmin. *Mol. Biol. Cell*. **10**, 105–118

9. K. K. Gupta et al. (2013) Mechanism for the catastrophe-promoting activity of the microtubule destabilizer Op18/stathmin. *Proc Natl Acad Sci USA*. **110**, 20449–20454
10. N. Larsson et al. (1999) Op18/stathmin mediates multiple region-specific tubulin and microtubule-regulating activities. *J. Cell Biol.* **146**, 1289–1302
11. D. L. Gard and M. W. Kirschner (1987) Microtubule assembly in cytoplasmic extracts of *Xenopus* oocytes and eggs. *J. Cell Biol.* **105**, 2191–2201
12. P. Amayed et al. (2002) The effect of stathmin phosphorylation on microtubule assembly depends on tubulin critical concentration. *J. Biol. Chem.* **277**, 22718–22724
13. J. Koppel et al. (1990) Developmental tissue expression and phylogenetic conservation of stathmin, a phosphoprotein associated with cell regulations. *J. Biol. Chem.* **265**, 3703–3707
14. P. A. Curmi et al. (1997) The stathmin/tubulin interaction in vitro. *J. Biol. Chem.* **272**, 25029–25036
15. S. Honnappa et al. (2006) Control of intrinsically disordered stathmin by multisite phosphorylation. *J. Biol. Chem.* **281**, 16078–16083
16. E. Charbaut et al. (2001) Stathmin family proteins display specific molecular and tubulin binding properties. *J. Biol. Chem.* **276**, 16146–16154
17. B. Gigant et al. (2000) The 4 Å X-ray structure of a tubulin:stathmin-like domain complex. *Cell*. **102**, 809–816
18. S. Chauvin et al. (2008) Palmitoylation of stathmin family proteins domain A controls Golgi versus mitochondrial subcellular targeting. *Biol. Cell*. **100**, 577–591
19. S. Ozon et al. (1997) The stathmin family - molecular and biological characterization of novel mammalian proteins expressed in the nervous system. *Eur. J. Biochem.* **248**, 794–806
20. R. Ravelli et al. (2004) Insight into tubulin regulation from a complex with colchicine and a stathmin-like domain. *Nature*. **428**, 198–202
21. Y. Y. Yip et al. (2014) Differences in c-Jun N-terminal kinase recognition and phosphorylation of closely related stathmin-family members. *Biochem. Biophys. Res. Commun.* **446**, 248–254
22. G. Kohlmaier et al. (2009) Overly long centrioles and defective cell division upon excess of the SAS-4-related protein CPAP. *Curr. Biol.* **19**, 1012–1018
23. T. I. Schmidt et al. (2009) Control of centriole length by CPAP and CP110. *Curr. Biol.* **19**, 1005–1011
24. C.-J. C. Tang et al. (2009) CPAP is a cell-cycle regulated protein that controls centriole length. *Nat. Cell Biol.* **11**, 825–831
25. L.-Y. Hung et al. (2004) Identification of a novel microtubule-destabilizing motif in CPAP that binds to tubulin heterodimers and inhibits microtubule assembly. *Mol. Biol. Cell*. **15**, 2697–2706
26. A. Cormier et al. (2009) The PN2-3 domain of centrosomal P4.1-associated protein implements a novel mechanism for tubulin sequestration. *J. Biol. Chem.* **284**, 6909–6917
27. V. Campanacci et al. (2022) Structural convergence for tubulin binding of CPAP and vinca domain microtubule inhibitors. *Proc Natl Acad Sci USA*. **119**, e2120098119
28. T. Krouglova et al. (2003) Fluorescence correlation spectroscopy analysis of the dynamics of tubulin interaction with RB3, a stathmin family protein. *FEBS Lett.* **546**, 365–368
29. V. Campanacci et al. (2019) Selection and characterization of artificial proteins targeting the tubulin α subunit. *Structure*. **27**, 497–506
30. J. M. Wagstaff et al. (2023) Diverse cytomotive actins and tubulins share a polymerization switch mechanism conferring robust dynamics. *Sci. Adv.* **9**, eadf3021
31. I. Mignot et al. (2012) Design and characterization of modular scaffolds for tubulin

assembly. *J Biol Chem*. **287**, 31085–31094
32. V. Campanacci et al. (2019) Insight into microtubule nucleation from tubulin-capping proteins. *Proc Natl Acad Sci USA*. **116**, 9859–9864
33. B. Gigant et al. (2013) Structure of a kinesin-tubulin complex and implications for kinesin motility. *Nat Struct Mol Biol*. **20**, 1001–1007
34. A. Sharma et al. (2016) Centriolar CPAP/SAS-4 imparts slow processive microtubule growth. *Dev. Cell*. **37**, 362–376
35. A. Nawrotek et al. (2014) Biochemical and structural insights into microtubule perturbation by CopN from *Chlamydia pneumoniae*. *J. Biol. Chem.* **289**, 25199–25210
36. M. Castoldi and A. V. Popov (2003) Purification of brain tubulin through two cycles of polymerization-depolymerization in a high-molarity buffer. *Protein Expr Purif*. **32**, 83–88
37. A. Nawrotek et al. (2011) The determinants that govern microtubule assembly from the atomic structure of GTP-tubulin. *J Mol Biol*. **412**, 35–42
38. L. Cao et al. (2014) The structure of apo-kinesin bound to tubulin links the nucleotide cycle to movement. *Nat Commun*. **5**, 5364

Supplementary Figures

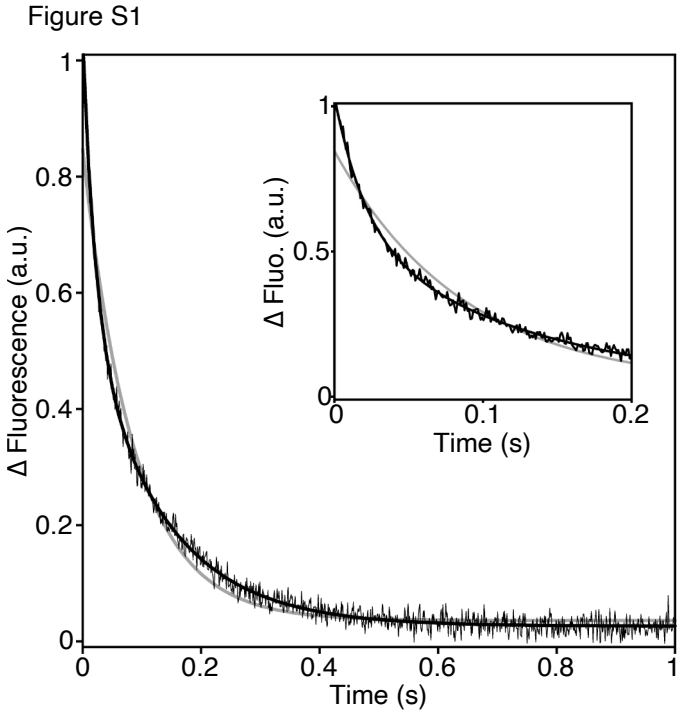

Figure S1. **Destabilization of the tubulin:R1 complex by PN2-3**. The experimental data from Fig. 2B (noisy curve) were fit with either a mono-exponential decay function (as in Fig. 2, grey curve) or a double-exponential decay function (black smooth curve). In this last case, the fit gives numerical k_{obs} values of 42 ± 6 s^{-1} and 7.4 ± 0.6 s^{-1}, which might correspond to a fast binding of PN2-3 to tubulin:R1 and to a slower dissociation of R1 from this transient ternary complex. (Inset) Close-up image of the first 0.2 s of the kinetics.

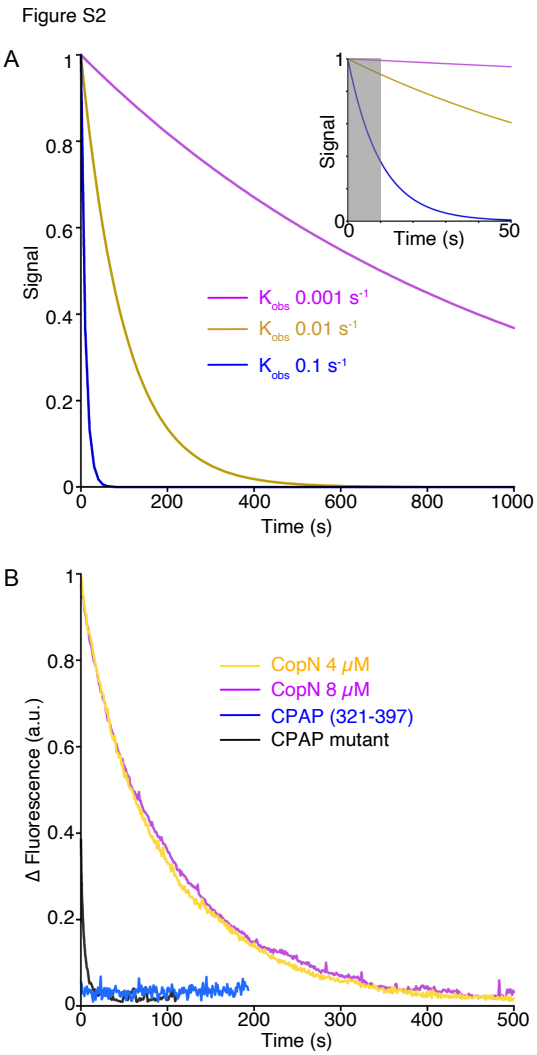

Figure S2. CPAP constructs destabilize T_2R more efficiently than CopN. (**A**) Theoretical mono-exponential decay curves for k_{obs}=0.001 s^{-1} (emulating T_2R dissociation in presence of excess unlabeled $RB3_{SLD}$; pink curve), k_{obs}=0.01 s^{-1} (approximating the chase by CopN; yellow), and k_{obs}=0.1 s^{-1} (blue). (Inset) Close-up image of the first 50 s of the theoretical kinetics. The first 10 seconds of the kinetics, which correspond to the time required for adding the protein competitor to the T_2R solution in the fluorescence cuvette and for mixing, are highlighted with a semi-transparent grey box. Therefore, k_{obs}=0.1 s^{-1} corresponds to the limit which can be detected in the assay with the spectrofluorometer and provides a lower bound of the k_{obs} for the destabilization of T_2R by CPAP constructs. (**B**) The difference in efficacity between CPAP constructs and CopN for T_2R destabilization is not related to their difference in affinity for tubulin or for T_2R. At time zero, 4 or 8 µM CopN (yellow or pink curve, respectively), or 4 µM CPAP 321-397 construct or its E323R-E324R-I327R triple mutant (blue or black curve, respectively) were added to fluorescent T_2R. Data for the 4 µM CopN concentration and for the wild type 321-397 fragment are from Fig. 3C.